Surface Composition of Stainless Steels during Anodic Dissolution and Passivation Studied by ESCA

I. Olefjord, B. Brox, and U. Jelvestam

Department of Engineering Metals, Chalmers University of Technology, S-412 96 Göteborg, Sweden

ABSTRACT

A molybdenum containing austenitic steel was exposed in hydrochloric acid at various potentials in the active and passive ranges of the alloys. The surface compositions were analyzed by the ESCA technique. The influence of pretreatment by ion bombardment and mechanical polishing on the passivation behavior was investigated. The passive film formed on the surface consists mainly of a mixed Fe-Cr-Mo oxide. The average content of Cr^{3+} in the oxide is about 70%. The inner layers of the oxide product consist mainly of Cr oxide. The Ni content in the oxide is low. The concentration and the chemical state of Mo is potential dependent. At low potentials in the passive range, the four-valency state is predominant, while at high potentials Mo exists mainly in its six-valency state. On the surface of the oxide, a layer of hydroxide is present. Chloride ions are incorporated into the passive film. The thickness of the passive film increases with the potential in the passive range from 10 to 15Å. The composition of the metal phase changes during active dissolution. Thus, the alloying elements are enriched on the surface and thereby control the dissolution rate, control overpotentials, and provoke passivation of the alloy.

Stainless steels belong to a class of metals and alloys which protect themselves by forming reaction products on their surfaces. The so-called passive film consists mainly of oxides, and its thickness is in many cases only a few atomic layers. The corrosion behavior of the steel is dependent on the properties of the passive film. The composition of the film is determined by the composition of the alloy and by the environmental conditions to which the steel is exposed. Exposure of the steel in chloride or other halogen ion environments may cause breakdown of the passive film followed by localized attack of the metal. Binary Fe-Cr alloys are especially susceptible to localized attack. By alloying these steels with Ni and Mo, the resistance against localized attack is markedly improved, but even high alloyed steels may be attacked in higher chloride containing acid solutions at least at elevated temperature. Thus, localized corrosion attack on stainless steels is one of the most serious problems in the use of these alloys. Therefore, it is important to clarify the factors controlling the chemical composition and the stability of the passive film.

By using surface-sensitive techniques (ESCA and Auger) (1-12) it has been possible in the past to get information about the composition of very thin reaction products formed on the surfaces. The ESCA method is unique in the sense that it gives information about the chemical state of the elements. The method allows us to estimate the thickness of the passive film due to the fact that the mean free path of the photoelectrons is of the same order of magnitude as the thickness of the film.

It has now been clarified that the passive film formed on austenitic steels consist mainly of Cr oxide, that the Ni content in the film is very low, and that Mo is present in the oxide. In earlier work (7, 10-12), it has been demonstrated that Fe is selectively dissolved during passivation. The alloying elements are thereby enriched on the surface in their metallic states.

The aim of this paper is to describe the surface condition of an austenitic stainless steel during its dissolution and passivation in a hydrochloride aqueous solution. Attention is directed to interpretation of the chemical states of the elements of the passive film and the distribution of chloride ions in the film.

Experiments

The polarization experiments were performed in an electrochemical cell connected to the preparation system of the ESCA instrument. Figure 1 shows a schematic view of the instrumentation. It consists of separate ESCA (HP 5950 A) and Auger (PHI 545) analyzers. The sample-preparation system allows simultaneous and independent analyses of both instruments. The electrochemical cell consists of a Teflon vessel with an opening to which the specimen is tightly screwed. A soft Teflon gasket prevents leakage. The cell is equipped with a Pt counterelectrode and an external reference electrode (SCE). The potential was controlled by a potentiostat (Wenking POS73). The solution was mechanically stirred in the cell and deaerated by argon bubbling. Before the electrolyte was used, it was deaerated by argon bubbling for 2h. The closed glass vessel in which the cell is located is streamed through by argon gas during the experiment and during transfer of the sample to the vacuum system. The arrangement is designed to minimize contact between the surface and oxidizing gases.

The steel used is a commercial austenitic stainless steel. Its composition, in weight percent, is: 0.040C, 0.62Si, 1.64Mn, 0.020P, 0.003S, 16.7Cr, 15Ni, 4.28Mo, 0.1Cu, 0.27Co, 0.27N, balance Fe. The electrolyte was 0.1*M* HCl + 0.4*M* NaCl. The samples were pretreated by polishing on emery paper to 600 grit finish and then electropolished in perchloric acid. Before exposure in the acid, the samples were either ion etched or mechanically polished on Al_2O_3 powder, grain size ~0.3 μm. The two different pretreatments were used to clarify their influence on the composition of the passive film.

Immediately after ion etching or grinding, the sample was fixed at the cell and the electrolyte was poured into the cell. The potential of the sample was applied in the following sequence: cathodic range, −450 mV for 10 min; corrosion potential for 5 min; cathodic potential −450 mV for 10 min; the chosen passive potential or corrosion potential. The dissolution at the corrosion potential was performed to dissolve the outer atomic layers of the metal and thereby obtain a surface state representing a self-corroding condition.

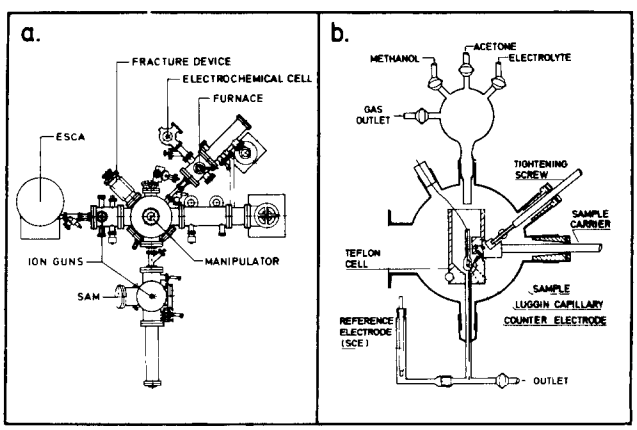

Fig. 1. a: The ESCA/Auger instrument. b: The electrochemical cell

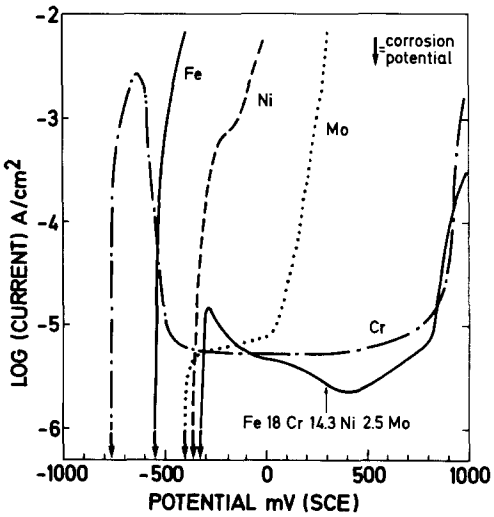

Fig. 2. Polarization diagrams

Anodic polarization curves were recorded in the test solution for the alloy and the pure metals Fe, Cr, Ni, and Mo. The samples were activated in the way described above and then swept in the anodic direction (20 mV/min). The anodic polarization curves are shown in Fig. 2. It appears that Cr is the only element which is passivated over a wide range in this solution. The passivation range of the alloy is almost as wide as for pure Cr. One difference between Cr and the alloy is that the maximum current density in the active range is about two orders of magnitude higher for Cr than for the alloy. Figure 2 also shows that Cr is the least noble of the elements. It also appears that the corrosion potential of the alloy is slightly higher than the corrosion potential of Ni and Mo.

Calibration

The chemistry of the passive film is very complex. The interpretation of the ESCA spectra, in particular Cr and Mo signals, is not straightforward. Therefore, the spectra of these elements recorded from pure metals, alloys, and compounds will be described in detail.

The metallic state of Cr $2p_{3/2}$ is shown in Fig. 3a. The two peaks, the solid and the point-dashed, are recorded from ion-etched pure metal and the alloy, respectively. The peak representing the pure metal is significantly narrower than the peak representing the Cr peak in the alloy. The full width at half maximum of the two peaks are 1.6 and 2.4 eV, respectively. The broadening is characteristic for the elements Cr and Mo in the alloy. The peaks in the spectra representing Fe and Ni in the same alloy are not broadened compared to the peaks obtained from the pure metals. This observation indicates that in an alloy containing Cr and Mo these alloying elements interact with each other in the surface region.

The spectra shown in this paper are the as-recorded signals. The signals are split into their components by using a gaussian/lorenzian distribution. For example, the solid and the dashed peaks in Fig. 3b represent the metallic and the oxide states of Cr, respectively. The solid inverse S-curve is the background, and the dotted curve is the sum of the background and the peaks representing the metallic and oxide states. The dotted curves are shown to demonstrate how well the deconvoluted states represent the recorded peak.

The rows b and c in Fig. 3 show the Cr and the oxygen spectra recorded after oxidation of pure Cr at 500°C in oxygen, 10^{-4} torr, for 0.5 and 5 min, respectively. The oxidation was performed in the preparation chamber. The short oxidation time gives an oxide that only partly covers the surface. The contribution from the metallic state of Cr, binding energy BE = 573.8 ± 0.2 eV, is easily readable. [The spectrometer is calibrated by setting the binding energies of carbon (graphite) and Ni to 284.3 and 852.8 eV, respectively.] The binding energy of the oxide state

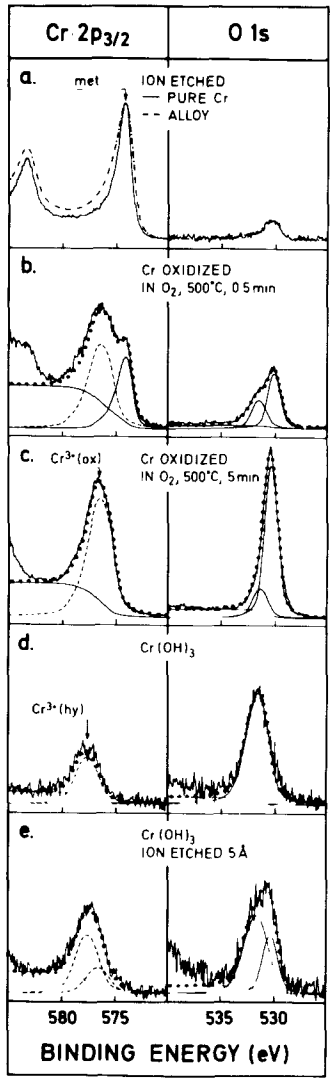

Fig. 3. ESCA spectra recorded from Cr and oxygen. a: Ion-etched pure Cr and Fe18Cr14.3Ni2.5Mo (a/o). b and c: Cr oxidized in O_2. d: $Cr(OH)_3$. e: $Cr(OH)_3$ ion-etched 5Å.

(dashed curve) is 2.5 eV higher than BE of the metallic state (the chemical shift). After oxidation for prolonged time (Fig. 3c), the surface is completely covered by the oxide. The position of the oxide state of Cr, BE = 576.3 eV, is the same as after oxidation for short time. The recorded oxygen signal consists of two peaks. The main peak at 530.0 eV corresponds to oxygen in Cr_2O_3, while the small peak at 531.4 eV represents oxygen in hydroxide.

Figure 3d shows the spectra recorded from $Cr(OH)_3$. This compound was produced from an aqueous solution, pH = 3, containing 0.01*M* $CrCl_3$ to which one droplet of concentrated NH_4OH was added. The solid product from the reaction, $CrCl_3(aq) + 3NH_4OH(aq) \rightarrow Cr(OH)_3(s) + 3NH_4Cl(aq)$, was allowed to settle on a gold support on the bottom of the reaction cup. After dilution and drying, the sample was moved to the ESCA instrument. The spectra show that the positions of Cr and oxygen signals are shifted to higher binding energies. The shifts compared to Cr_2O_3 are 0.8 and 1.4 eV, respectively. The ratio between the intensities of oxygen and Cr^{3+} is 1.5. This is about twice as much as obtained from the Cr oxide. The difference in chemical shifts for Cr^{3+} and oxygen in oxide and hydroxide gives information on the structure of the passive film. However, as shown in Fig. 3e, a slight ion etching of $Cr(OH)_3$ noticeably changes the spectra: extra peaks appear on the low binding energy sides of the main peaks; the positions of these peaks correspond to the positions of Cr^{3+} and O^{2-} in Cr_2O_3. Thus, ion etching of $Cr(OH)_3$ decomposes it to Cr_2O_3. [SiO_2 is used as cali-

brating compound for the ion etching rate.] Prolonged ion etching increases the relative amount of transformed compounds and gradually a stationary state is reached. After ion etching to 100Å below the original surface, the intensity of the signal corresonding to the oxide state is three times higher than the intensity of the hydroxide state. This experiment has been reported earlier (3). In that case, it was also shown that heating of $Cr(OH)_3$ in vacuum causes the same effect as ion etching. In this study, it was also found that $Cr(OH)_3$ is transformed to Cr_2O_3 when bombarded with low energy electrons (10 eV) from a flood gun (normally used for neutralizing the surface of an insulator during ESCA analysis).

Figure 4 shows Mo 3d and signals recorded from pure Mo and oxide products. The binding energy of Mo $3d_{5/2}$ in its metallic state is 227.4 eV. The full width at half maximum is 1.0 eV. From the alloy, the corresponding width is 1.2 eV. The spectra in the rows b and c were obtained after oxidation in dry oxygen and H_2O vapor, respectively. Oxidation in pure oxygen, 1 torr, at 400°C for 10 min gives MoO_3. The binding energy of the six-valency state of Mo $3d_{5/2}$ is 232.2 eV (chemical shift is 4.8 eV). Oxidation in H_2O vapor gives a completely different spectrum. Figure 4c shows the signals recorded after oxidation in H_2O vapor, 1 torr, at 720°C. The position of the peak at BE = 229 eV, marked Mo^{4+}, is found to be the same as in MoO_2. The signal marked "hy" is an extra peak located between the six- and the four-valency states of Mo. The binding energy of this state is 230.6 eV. (Chemical shift is 3.2 eV.) It is broader than the Mo^{4+} and the Mo^{6+} signals. The position of the peak representing the four-valency state is strongly dependent on the coordination of the Mo^{4+} ions. Thus, it is expected that Mo^{4+} peaks recorded from pure MoO_2 and from a mixed oxide containing Mo^{4+} are not situated in the same positions. It was suggested in Ref. (12) that the Mo^{hy} peak represents the four-valency state in an oxyhydroxide. Indications underlying this statement are the broadening of the peak and the shift of its position. The latter is characteristic for hydroxide, for example, $Cr(OH)_3$ discussed above and $Ni(OH)_2$ (13). An extensive study of the oxides of Mo will be published later (14).

The composition and the thickness of the passive film were obtained from the expressions (11)

$$I_M^{ox} = D_M^{ox} S_M^{ox} (1 - \exp[-\alpha^{ox}/(\lambda_M^{ox} \sin 38.5)]) \exp(-\alpha^c/[\lambda_M^{ox} \sin 38.5]) \quad [1]$$

$$I_M^{met} = D_M^{met} S^{met} \exp[-(\alpha^{ox} + \alpha^c)/(\lambda_M^{ox} \sin 38.5)] \quad [2]$$

$$C_M^{ox} = D_M^{ox}/\Sigma D_N^{ox} \text{ alt. } C_M^{met} = D_M^{met}/\Sigma D_N^{met} \quad [3]$$

where I^{ox} and I^{met} are the measured intensities from the element M in the oxide and metal phases. D is the density of the element; S the relative photoelectron yield factor, experimentally determined, taking into account geometrical and attenuation factors; λ the attenuation length of the photoelectrons (11); α^{ox} and α^c the thicknesses of the passive film and the contamination layer, respectively.

The attenuation of the photoelectrons due to the contamination is taken into account individually for each sample by measuring the intensities of the metal elements before and after a slight ion etching of the surface, which just removes the contaminants. Then, the thickness of the contamination layer, α^c, is calculated from Eq. [2]. The thickness of the passive film, α^{ox}, is estimated from Eq. [1] and [2].

Results

Figure 5 illustrates ESCA spectra recorded from the sample after polarization in 0.1*M* HCl + 0.4*M* NaCl. The spectra in the three rows were recorded after 5 min at the corrosion potential (Fig. 5a) and 1h at the passive potentials −100 mV and +500 mV (SCE) (Fig. 5b and 5c, respectively). The alloying elements—Ni, Fe, Cr and Mo— are present in their metallic states. Except for Ni, they are also oxidized. Even when the sample was treated at the

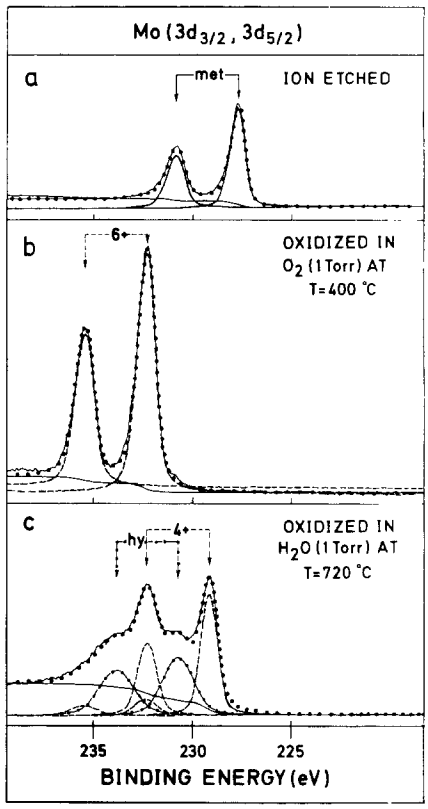

Fig. 4. ESCA spectra recorded from Mo. a: Ion-etched. b: Oxidized in O_2 c: Oxidized in H_2O vapor.

dissolution potential (−320 mV) for 5 min, oxide products are present on the surface. It is suggested that these are formed during rinsing and transferring of the sample to the analyzer. The oxide film is extremely thin; its thickness, estimated by the formula above, is 4Å. The cations in the film correspond to oxidation of less than one atomic plane of the metal.

The ESCA spectra recorded are deconvoluted by using the positions and peak widths obtained from the calibration study, except in the case of the metallic state of Cr, Ni, and Mo, because these signals are broadened when they are recorded from alloys containing these elements.

After passivation, the Cr^{3+} peak is the strongest of the peaks representing the oxidized states. From the figure, it appears that two oxide peaks representing Cr-hydroxide and Cr-oxide are present. The hydroxide state (chemical shift of 3.3 eV) is dominating at −320 and at −100 mV. Iron is present as Fe^{2+} and Fe^{3+}. The intensity of the latter is the strongest. The obtained intensity ratios, $Fe^{2+}/(Fe^{2+} + Fe^{3+})$, are 0.30 ± 0.09, 0.44 ± 0.03, and 0.40 ± 0.07 at the three potentials (−320, −100, and +500 mV *vs.* SCE). Thus, due to the uncertainty it is not possible to conclude about the changes of the valency-state ratio of Fe in the passive state.

The deconvolution of the Mo spectra is shown in Fig. 6. It appears that, in spite of the fact that the spectra are broad with no distinct peaks, the set of Mo states described above satisfy the recorded peaks very well. The oxide state of Mo is dependent on the passivation potential. At low potential, the dominating state is the four-valency state, while at high potential the contribution from the six-valency state is more pronounced. It also appears from Fig. 6 that the peak representing the metallic state is broader than the pure metal state. This is suggested to be due to strong interaction between Mo and the alloying elements Ni and Cr.

In Fig. 5 the metalloids oxygen, carbon, and chlorine are also shown. The main origin of carbon is acetone and methanol, in which the surface was rinsed. The three peaks correspond to the bondings C—H, C—OH, and C═O. The oxygen signal also consists of three peaks. That at low binding energy corresponds to O^{2-} in the ox-

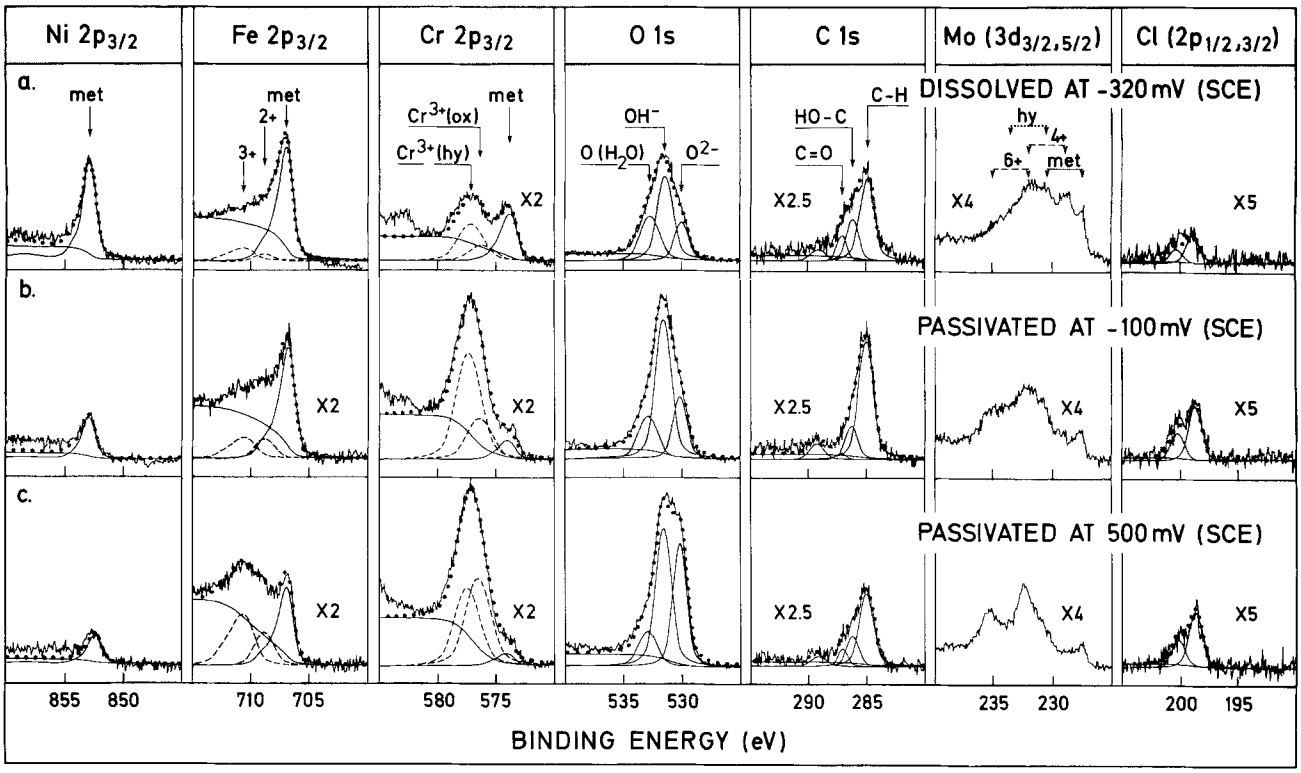

Fig. 5. ESCA spectra of the Fe18Cr14.3Ni2.5Mo alloy recorded after polarization. a: Active range, −320 mV (SCE). b: Passive range, −100 mV (SCE). c: Passive range, +500 mV (SCE).

ides Cr_2O_3, MoO_2, and Fe_2O_3. The peak denoted OH^- has the same position as oxygen in $Cr(OH)_3$ and Mo-hydroxide. This peak overlaps with the signal from the OH group of methanol. The third peak represents water as well as oxygen in acetone. The samples polarized at the dissolution potential were treated in acetone only. The passivated samples were rinsed in acetone and methanol. The difference in rinsing treatment can be read from the figure. It appears that the oxygen peaks recorded after passivation are narrower than after dissolution. This shows that methanol completely removes acetone from the surface, but, on the other hand, this also implies that water bonded in the passive film could be removed. In interpretation of the oxygen signals, the intensity of the peaks representing OH^- and H_2O are reduced by the contribution from methanol and acetone. The contribution is estimated to be $2.5 \times I(C)$, where $I(C)$ is the intensity of the corresponding carbon peak (C—OH or C=O). It appears from the figure that Cl^- ions (BE = 198.5) are present in the oxide product. No Na^+ ions were detected; thus, Cl^- ions are not bound as salt crystals on the surface. Later, it will be shown that the Cl^- ions are incorporated in the film.

Figures 7-11 show the results obtained from quantitative evaluation of the ESCA spectra. The data obtained are given for each individual experiment at the dissolution potential −320 mV and the passive potentials −100 and +500 mV. The notations MP and IE refer to the pretreatments, mechanical polishing and ion-etching, respectively. The cation contents in Fig. 7 are calculated from the intensities obtained in the as-polarized condition, *i.e.*, before ion etching. Thus they do not take into account any in depth variations of the composition. Furthermore, all oxide states are summed.

The passive films formed at −100 and +500 mV (SCE), polarized for 1h (Fig. 7), consist mainly of Cr^{3+} compounds (oxide and hydroxide). The Cr^{3+} content is about 70%. It seems to be constant and does not vary with the potential. The measured Fe^{ox} (Fe^{2+} and Fe^{3+}) content is in the range 20 to 25 atom percent (a/o) at −100 mV (SCE) and slightly higher at +500 mV (SCE). The higher Fe^{ox} concentration at +500 mV compensates for the lower Mo^{ox} content at this potential. The measured Mo^{ox} is 7-9 a/o at −100 mV (SCE) and about 5 a/o at the higher potential. It appears from the figure that the cation content is independent of the pretreatment of the surface. It could be expected that the Mo content of the samples pretreated by ion etching should be higher because ion etching causes enrichment of Mo on the surface due to the lower sputtering rate of Mo.

The oxide products formed on the surface during rinsing and transferring of the polarized sample to the dissolution potential, −320 mV (SCE), depend on the pretreatment procedure. Figure 7 shows that the mechanically polished (MP) samples polarized for 5 min at the dissolution potential consist mainly of Fe^{ox}. The Cr^{3+} is only 35 a/o, which is half of the value obtained after passivation. The Mo^{ox} content is about 15 a/o, which is twice as much as obtained after passivation at −100 mV. The samples prepared by ion etching and polarized for 5 min show much higher Cr^{3+} contents (52 and 55 a/o) The Fe^{ox} and Mo^{ox} concentrations are about 35 and 10 a/o, respectively. Polarization for 1h gives about the same result. It is suggested that the high Cr^{3+} content in the film is indirectly an effect of the ion etching. The etching causes enrichment of Mo on the surface and makes it impossible to keep the surface in its active state; instead, it is passivated.

The thicknesses of the surface oxide products are shown in Fig. 8. It appears that the thickness of the passive film increases with the potential. The values at −100 and +500 mV (SCE) are 10 and 15Å, respectively. After treatment at the dissolution potential, the thickness of the oxide formed on the mechanically polished surface is 5 ± 1Å. The average value of the ion-etched samples is about 40% higher.

Figure 9 shows the measured Cl^- ion content *vs.* the thickness of the oxide layer. The values are given before and after a slight ion etching. The ion etching was performed to establish whether the Cl^- ions were adsorbed on the surface or bonded in the oxide. The results show that Cl^- ions are found in the oxide. The figure indicates that at the corrosion potential the highest Cl^- content occurs on the surface covered with the thinnest oxide. The content of Cl^- ions increases with the potential in the passive range. The distribution of Cl^- ions through the

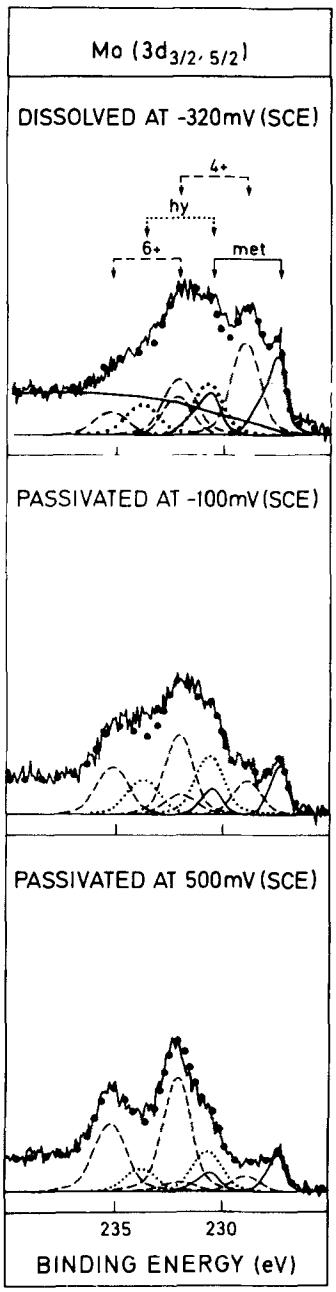

Fig. 6. Deconvoluted ESCA spectra of Mo from Fig. 5

passive film, obtained from ion etching, is shown in Fig. 10. Neglecting selective sputtering effects, it appears that the highest Cl^- concentration exists in the outer layer of the film.

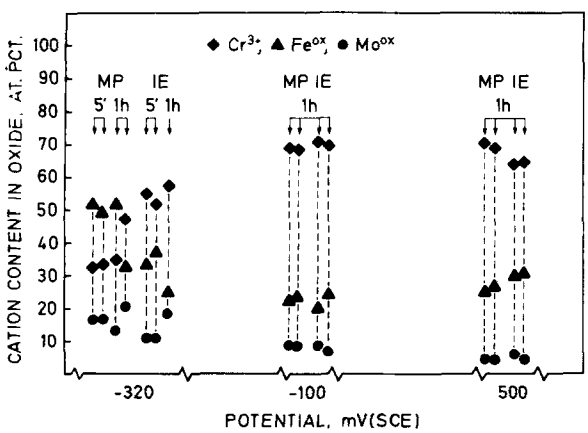

Fig. 7. The cation contents of the reaction products formed at −320 mV (SCE) and of the passive films formed at −100 mV (SCE) and at +500 mV (SCE).

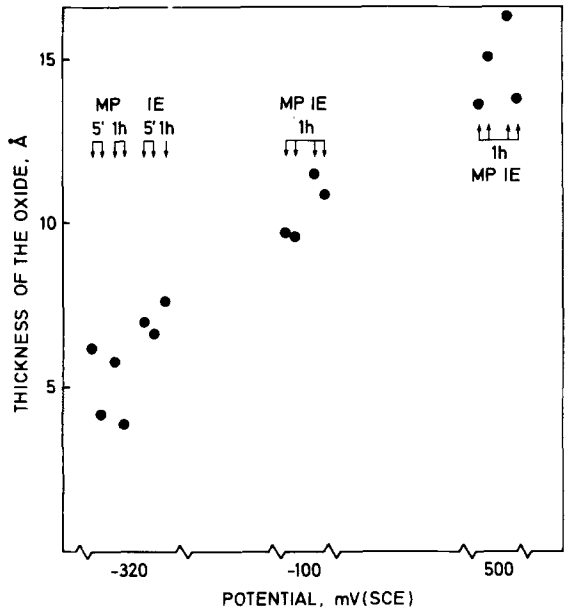

Fig. 8. Thickness of the oxide product vs. the potential

Figure 11 shows distribution of the ions through the passive film obtained by polarization to +500 mV (SCE). All Mo concentrations are multiplied by a factor of 10. The data points are average values from four measurements. Before ion etching, the difference between the total charges of cations and anions is less than 2%. The most characteristic feature of the figure is the high OH^- concentration in the outer layer. After ion etching, the OH^- content decreases and the O^{2-} increases. However, it has been demonstrated above that this is at least partly an artifact due to ion etching. It also appears that the outer layer contains hydration water. The profile shows that Cr^{3+} is the dominating species in the inner layer of the passive film. That this result should be an artifact can be excluded because prolonged sputtering into the bulk of the alloy with oxygen present in the sputtering gas (low pressure) gives a ratio between Fe^{ox} and Cr^{3+} which is almost identical to the alloy composition. The profile shows that Fe^{2+} is mainly present in the outer "hydroxide" phase. The content of Fe^{2+} in the inner layer may be an effect of the ion etching because Fe^{3+} is partly reduced to Fe^{2+}. It is suggested that the low Fe^{2+} content in the inner layer is not due to the fact that Fe^{2+} is reduced to the

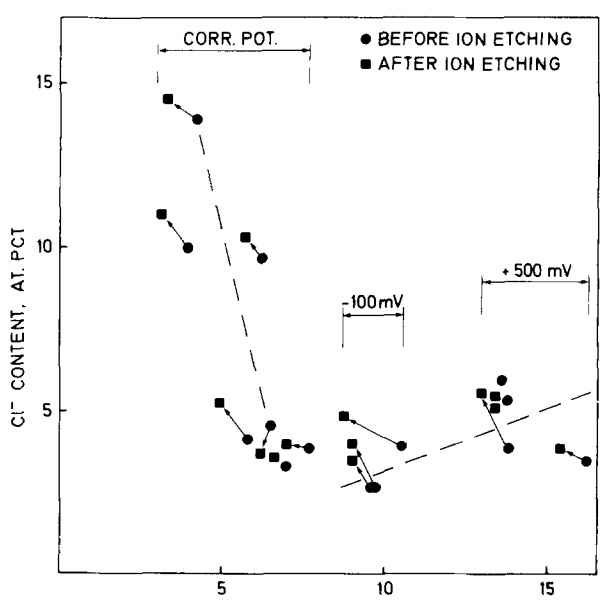

Fig. 9. Cl^- ion content vs. the thickness of the oxide product

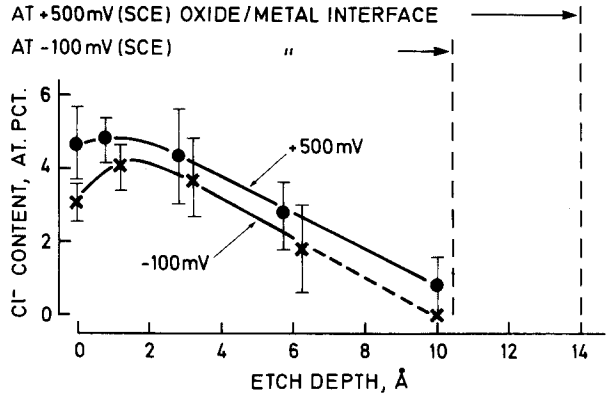

Fig. 10. Cl^- distribution at −100 mV (SCE) and at +500 mV (SCE)

metallic state of Fe because, in our experimental setup, we have never observed reduction of Fe^{3+} via Fe^{2+} to Fe^{met}. The Mo content in the passive film is less than 2%. At this potential, Mo is mainly present in the outer layer as Mo^{6+}, while at low potential Mo^{4+} is dominating. Both Fe and Mo are detected in the inner layer of the oxide.

Due to the fact that the oxide products on the alloy are very thin, it is possible to get information about the composition of the metallic state underneath the oxide. The dots in Fig. 12a mark the calculated (by using the formulas [2] and [3]) composition of the metal phase after polarization to the corrosion potential of the sample. The composition obtained is apparent because the formulas [2] and [3] do not take into account the real distribution of the alloying elements in the surface region. The solid bars show the bulk composition of the alloy. It appears from the figure that the apparent Fe concentration is about 10 a/o units lower than the Fe content of the alloy. It also shows that Ni is markedly enriched in the surface region because the apparent Ni content is about twice as high as the figure given from the chemical analysis of the alloy. Furthermore, Mo is slightly enriched, while Cr is depleted in the surface region.

Above, it has been emphasized that the oxide products present on the surface after polarization to the corrosion potential are mainly formed during rinsing and transferring of the sample. It is suggested that the depletion of Cr in the metal phase is caused by selective oxidation during handling of the sample because the Cr

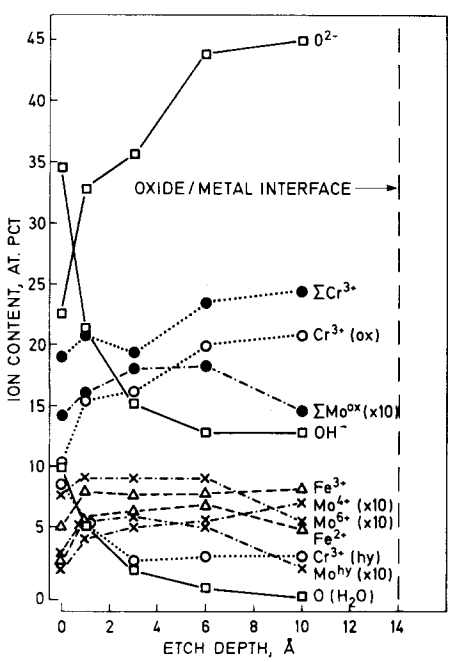

Fig. 11. Ion content vs. etch depth at +500 mV (SCE)

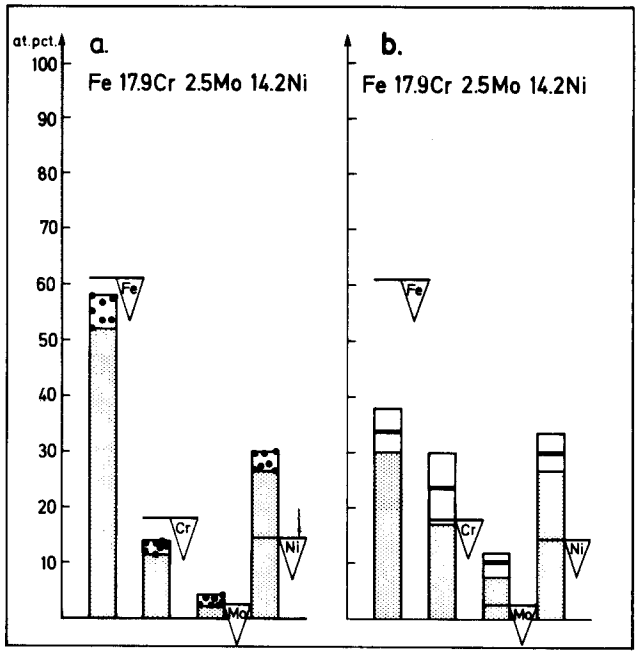

Fig. 12. The composition of the metal phase during dissolution at active potential. a: The apparent metal content. b: The estimated metal content in the outermost atomic layer (15).

content in the oxide is higher than in the alloy. Iron, on the other hand, shows lower concentration in both the oxide and the metal phases compared to the bulk concentration. This observation shows that Fe is dissolved selectively during dissolution at the corrosion potential. Thereby the alloying elements are enriched on the surface.

The observation that Fe is selectively dissolved during dissolution of stainless steel in the active range of the alloy has been reported earlier (10-12). An extensive analysis of the distribution of the alloying elements in the neighborhood of the surface is given in Ref. (15). In that paper, the cations present in the oxide were converted to their metallic state. Also, it was assumed that the alloying elements differ from the bulk concentration in the three outer atomic planes.

The composition of the outermost atomic plane is shown in Fig. 12b [using the procedure in Ref. (15)]. The solid lines in each bar show the average value, while the white area is the standard deviation. The figure shows that during anodic dissolution the alloying elements Cr, Ni, and Mo are significantly enriched in the surface region.

In Fig. 13, the precision of the quantitative method is demonstrated. The alloy was polished on emery paper in methanol and transferred to the analyzer. It is suggested that no selective dissolution of the alloy occurs during polishing in methanol. The apparent composition is shown in Fig. 13a. The cations in the oxide (8Å) formed during transfer were converted to their metallic state, and the composition of the outermost layer was calculated (Fig. 13b). The calculated concentration of the alloying elements in the outermost atomic plane in this case is very close to the bulk composition of the alloy. Thus, the enrichment of the alloying elements during active dissolution of the alloy is a real effect.

Discussion

This study confirms the duplex structure of the passive film with an outer layer of hydrated hydroxide and an inner layer of oxide. The thickness of these layers cannot be determined exactly, but the sputtering profiles of oxygen in OH^- and H_2O states show that the hydroxide layer is at least one third of the whole film. Both layers consist of mainly Cr^{3+} compounds. Of the total cation content, the content of Cr^{3+} is at least 70 a/o. Nickel in its oxide state cannot be detected in the passive film. Iron is

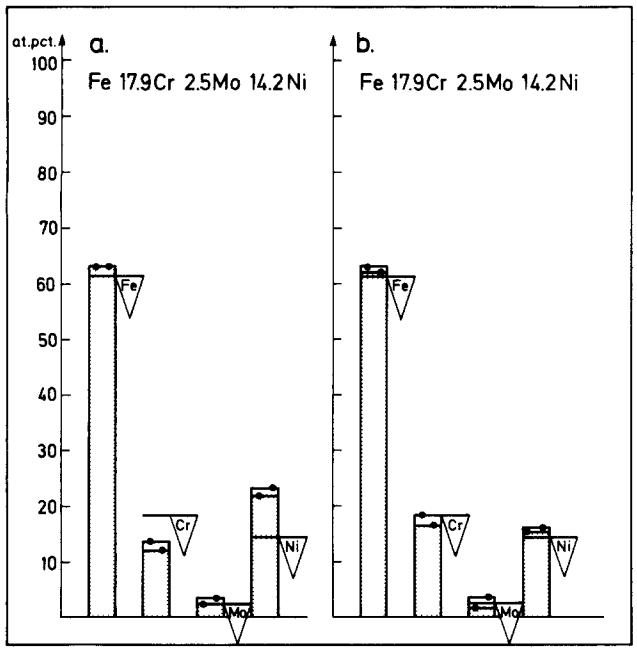

Fig. 13. The austenitic steel polished on emery paper in methanol. a: The apparent content b: The estimated composition of the outermost layer (15).

present in its di- and tri-valent states. The molybdenum content in the passive film is low, a few atomic percent. At −100 mV (SCE), the Mo four-valency state is dominant, while at +500 mV (SCE) Mo is present mainly as Mo^{6+}. The oxidation states of both Mo and Fe are reduced during ion etching. Considering the above, it can be concluded that the inner oxide layer consists mainly of Cr and Fe in their three-valency states.

The analysis shows that Cl^- ions are present in the surface products. The amount increases with the potential in the passive range. A suggested explanation for this behavior is that the field strength is higher at the high potential, even in spite of the fact that the layer is thicker. The incorporation of Cl^- in the film is completely different from the situation when stainless steel is exposed in sulfuric acid (12). In that case, SO_4^{2-} ions are merely adsorbed on the surface and completely removed by a slight ion etching. The difference in behavior is suggested to arise from the fact that the Cl^- ion is the same size as the OH^- ion and, therefore, can easily be substituted in the outer hydroxide layer.

The role of Mo has been discussed in the literature. Sugimoto *et al.* (6, 16) and Hashimoto *et al.* (8, 9) suggest that the stability of the oxide film in acid chloride solutions is the result of hexavalent molybdenum oxide forming on the surface. Hashimoto explains the fact that Mo alloyed steels show a much lower current in the passive region by a model in which the passive film is not homogeneous; instead, it contains a high density of microcracks through which current can leak. The microcracks are filled with water, and this is responsible for the high current. In the case of Mo-alloyed steels, Mo^{6+} ions are formed in the cracks and thereby decrease the size of the active sites. It was also mentioned that this Mo^{6+} compound is formed on the surface during active dissolution preceding passive film formation. This idea is to some extent contradictory to the results reported in this study. It has been shown that the six-valency state of Mo is obtained at high potential. At low potential, Mo^{4+} dominates. Also, comparing the result from passivation of pure Mo (17) no six-valency Mo compound is found at potentials lower than +250 mV (SCE). However, from a thermodynamic point of view (18), Mo^{6+} is expected even at lower potentials; Mo is oxidized to MoO_3 above −182 mV and to MoO_4^{2-} above −242 mV (SCE) (standard conditions). Interpretation of these compounds by ESCA is not an easy task due to the fact that the positions of the signals representing Mo in the compounds are very close to each other.

Our result indicates that Mo is uniformly distributed through the layer. Support for this statement is that the high energy peak of the complex Mo^{4+} signal is dominating after passivation and that both Mo^{4+} and Mo^{6+} exist through the layer. We suggest that the role of Mo in the passive film is that it stabilizes the oxide products. At least the outer hydroxide layer is influenced. It is known that some Mo complexes [*i.e.*, $Mo_3Cl_4(H_2O)_2(OH)_2\ 6H_2O$] are insoluble in acid while corresponding Fe-Cr-compounds are soluble. It has been suggested by Wanklyn (19) that hydrated MoO_2 occurs in the passive film. We conclude that the outer part of the passive film consists of a mixed hydroxide containing Mo, Fe, and Cr. The latter is directly observed in the spectra.

We have reported (12) that in the case of ferritic steels exposed in 0.5*M* H_2SO_4 the passive film consists almost entirely of Cr_2O_3 in the inner layer. It was suggested that it is this inner oxide layer that is rate determining for the dissolution. The observation that the oxide consists of mainly three-valency cations implies that the defect density of the passive film is low. However, both lower (Fe^{2+}) and higher (Mo^{4+} and Mo^{6+}) valency cations are present in the film. It is suggested that the defects created by Fe^{2+} are canceled by the defects created by Mo^{4+} and Mo^{6+} Thus, an almost defect-free oxide is formed in which ionic conductivity is extremely low.

It is found that the thicknesses of the passive films formed on this austenitic steel in hydrochloric acid (0.1*M* HCl) and on a Mo containing ferritic steel (12) in sulfuric acid (0.5*M* H_2SO_4) follow the same potential dependence. Even the absolute thickness is almost the same. In the case of non-Mo containing steel (12), the film was noticeably thicker at low potential. Thus, the thickness of the passive film seems mainly to be dependent on the Mo content in the alloy.

At the dissolution potential of the alloy, the alloying elements Ni, Cr, and Mo are enriched on the surface in their metallic states. The enrichment is caused by selective dissolution of Fe. The high Ni content is directly observed from the measurements. The contents of Cr and Mo were obtained by converting the cations in the oxide to their metallic states. It was not possible to avoid a slight oxidation of the surface during handling in spite of all precautions taken. It could be argued that Cr in its oxide state is present on the surface even during active dissolution because pure Cr is passive at the dissolution potential of the alloy (Fig. 2). However, even Fe and Mo are present as oxide on the surface after the dissolution treatment. Iron is the dominating cation in the oxide product, but pure Fe is definitely not passive at the corrosion potential of the alloy. A further indication for the statement that most of the oxide is formed after polarization is that the oxide product formed on the surface of an etched sample in the protecting atmosphere of the cell is thicker than the products discovered after polarization to the corrosion potential.

The selective dissolution of Fe is controlled by the interatomic forces over the interface (metal/solution) and between the alloying elements. Earlier (11), it has been suggested that the elements form a surface phase with lower Fe content than the bulk composition of the alloy. The alloy system forms at high temperature intermetallic compounds (σ-, X-, and Laves phases). During active dissolution, corresponding phases are suggested to be formed due to interaction between the atoms. The initiation of the enrichment is described by the model: at the corrosion potential of the alloy, the dissolution rates of Fe and Cr are higher than the dissolution rate of Mo and Ni because Fe and Cr are less noble than Mo and Ni; interatomic forces between Cr and Mo slow down the dissolution rate of Cr, and thereby it is enriched on the surface. After the initiation, a steady state is reached where the overall dissolution rate is lowered.

The analysis shows that the thickness of the passive film increases with the potential in the passive region.

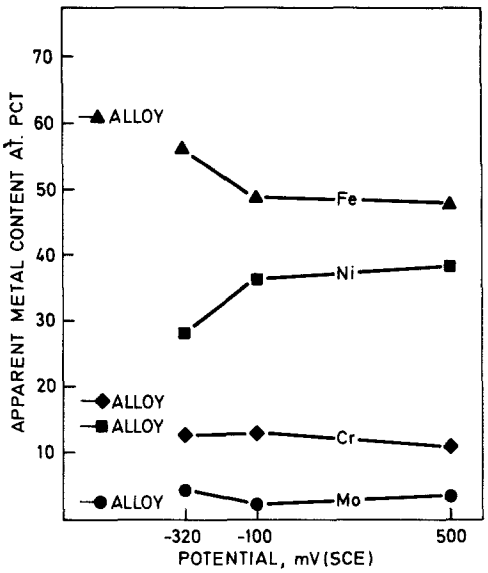

Fig. 14. The apparent metal content of the alloy *vs.* the potential (SCE).

Because Ni is not present in the oxide (or to only a low extent) and dissolves with a lower dissolution rate than Fe, it is enriched under the passive film. Figure 14 shows the apparent composition of the metal phase. It appears that the apparent Ni content is about twice as high as the bulk composition and that it increases with the potential. Because the excess of Ni atoms is located in a few atomic planes close to the oxide/metal interface, the Ni content of the outermost of these is higher than the value given in the figure.

Because all electrochemical reactions between the metal and the environment take place in the outermost atomic plane, the surface composition and the surface state contribute to the overall reactions and control factors as dissolution rate, overpotential, corrosion potential, and passivability. From the polarization diagram, Fig. 2, it appears the corrosion potential of the alloy is close to the corrosion potential of pure Mo and Ni. It has been emphasized that one beneficial effect of Mo and Ni is the enrichment of these elements on the surface during the anodic dissolution (10, 11, 15) that always precedes passivation. Thereby, the dissolution rate is lowered and the passivation of the alloy is provoked.

Conclusions

The passive film formed on a Mo containing austenitic steel consists of Cr oxide containing Mo and Fe. Chromium is present in hydroxide and oxide compounds. The Ni content of the film is very low. The valency states of Mo are Mo^{4+} at low potentials and Mo^{6+} at high potentials. Chloride ions are incorporated into the oxide passive film. The alloying elements Cr, Ni, and Mo are enriched on the surface during active dissolution. The enrichment is caused by selective dissolution of Fe. The enrichment of the alloying elements provoke passivation of the alloy.

Acknowledgment

The authors gratefully acknowledge the Swedish Board of Technical Development for financial support.

Manuscript submitted April 15, 1985; revised manuscript received Aug. 22, 1985. This was Paper 234 presented at the New Orleans, Louisiana, Meeting of the Society, Oct. 7-12, 1984.

Chalmers University of Technology assisted in meeting the publication costs of this article.

REFERENCES

1. I. Olefjord, in "Proceedings of the 6th Scandanavian Corrosion Congress," p. 11, Swedish Corrosion Institute, Stockholm (1971).
2. H. Fischmeister and I. Olefjord, *Monatsh. Chem.*, **102,** 1486 (1971).
3. I. Olefjord and H. Fischmeister, *Corros. Sci.*, **15,** 697 (1975).
4. J. E. Castle and C. R. Clayton, *ibid.*, **17,** 7 (1977).
5. B-O. Elfström, *Mater. Sci. Eng.*, **42,** 173 (1980).
6. K. Sugimoto and Y. Sawada, *Corros. Sci.*, **17,** 425 (1977).
7. I. Olefjord and B-O. Elfström, in "Proceedings of the 8th International Symposium on Reactivity of Solids," J. Wood, O. Lindquist, C. Helgesson, and M.-G. Vannerberg, Editors, p. 791, Plenum Press, New York (1977).
8. K. Hashimoto, K. Asami, and K. Teramoto, *Corros. Sci.*, **19,** 3 (1973).
9. K. Hashimoto, and K. Asami, *ibid.*, **19,** 251 (1979).
10. I. Olefjord, *Mater. Sci. Eng.*, **42,** 161 (1980).
11. I. Olefjord and B-O. Elfström, *Corrosion (Houston)*, **38,** 46 (1982).
12. I. Olefjord and B. Brox, in "Passivity of Metals and Semiconductors," M. Froment, Editor, p. 561, Elsevier Science Publishers, Amsterdam (1983).
13. P. Marcus, J. Oudar, and I. Olefjord, *J. Microsc. Electron.*, **4,** 63 (1979).
14. B. Brox and I. Olefjord, *Corros. Sci.*, To be published.
15. B. Brox and I. Olefjord, in "Stainless Steel 84," p. 134, The Institute of Metals, London (1985).
16. K. Sugimoto and Y. Sawada, *Corrosion*, **32,** 347 (1976).
17. B. Brox and I. Olefjord, *Corrosion (Houston)*, To be published.
18. A. A. Pozdeeva, E. I. Antonovskaya, and A. M. Sukhotin, *Prot. Met.*, **1,** 15 (1963).
19. J. N. Wanklyn, *Corros. Sci.*, **21,** 211 (1981).